Journal of Applied Fluid Mechanics, Vol. 18, No. 12, pp. 2941-2952, 2025.
Available online at www.jafmonline.net, ISSN 1735-3572, EISSN 1735-3645.
https://doi.org/10.47176/jafm.18.12.3522

Surrogate-assisted Multi-component Aerodynamic Optimization of Centrifugal Compressor Towards Performance Improvement of Adaptive Cycle Engine

A. Anjomrouz[1], W. Zou[2], W. Kong[2], B. Wang[2] and X. Zheng[3†]

[1] *Department of Mechanical Engineering, Sharif University of Technology, Tehran, 1458889694, Iran*
[2] *Institute for Aero Engine, Tsinghua University, Beijing, 100084, China*
[3] *State Key Laboratory of Automotive Safety and Energy, School of Vehicle and Mobility, Tsinghua University, Beijing, 100084, China*

†*Corresponding Author Email: zhengxq@tsinghua.edu.cn*

ABSTRACT

Centrifugal compressors are widely used in gas turbines, so it's important to have an efficient performance; also, optimizing this part can affect the whole engine's performance. Adaptive Cycle Engines (ACEs) are a group of gas turbine engines that can change key aerodynamic parameters such as pressure and bypass ratio through geometric structure adjustment. In the present research, the ACE with a centrifugal compressor as its high-pressure compressor (HPC) is investigated, and the aim is to improve the engine performance through compressor optimization. A three-dimensional surrogate-assisted aerodynamic optimization method is applied to maximize the isentropic efficiency of the centrifugal compressor with a constraint on the total pressure ratio. The optimization results show a 3.4% improvement in the design point efficiency, a 1.4% increment of the choked mass flow rate, and a wider operating range is obtained. Afterward, thermodynamic modeling of the engine performance is used to calculate the engine characteristics before and after the optimization. 3D performance maps of the compressor and fan, calculated by CFD simulation, are used for accurate engine performance modeling. The final results of the engine performance show a reduction of 2.0% in the specific fuel consumption of the improved engine, which is an important achievement in these engines.

Article History

Received March 13, 2025
Revised May 29, 2025
Accepted July 4, 2025
Available online October 6, 2025

Keywords:

Centrifugal compressor
Adaptive cycle engine
Aerodynamic optimization
Efficiency
Specific fuel consumption

1. INTRODUCTION

Centrifugal compressors are an important group of turbomachines widely used in gas turbines in military and civil applications, including aircraft propulsion, marine, and land transportation, power generation, etc. (Saravanamuttoo et al., 2017; Anjomrouz et al., 2023;). Because of these wide applications, the design optimization of these compressors is important. Nowadays, high efficiency, high pressure ratio, dimension minimization, and broad operating range are the common goals of compressor design optimization problems (Cheng et al., 2019; Xiang et al., 2021). In recent years, the design optimization of centrifugal compressors has been discussed in some research.

Verstraete (2010) developed a computer-aided design and optimization (CADO) tool for turbomachines. Application of the inverse design method in centrifugal compressor optimization and modification is investigated in (Zangeneh et al., 1999; Nili-Ahmadabadi & Poursadegh, 2013a, b). Mojaddam and Moussavi (2017) studied the design and optimization of the meridional profiles of the centrifugal compressor impeller by comparing the circular and elliptical curves for the meridional profile. They found that the elliptic curves can be a better initial selection. Mojaddam and Pullen (2019) optimized a centrifugal compressor of a turbocharger. They used the Design of Experiments (DoE), Box-Behnken design, and response surface method to increase the efficiency and pressure ratio by 3% and 11%, respectively. Hehn et al. (2018) applied the aerodynamic optimization of a transonic centrifugal compressor with the genetic algorithm (GA) and artificial neural networks (ANN) to increase isentropic efficiency and reduce acoustic effects. The optimization process was done for three operating points on the constant speed line corresponding to the design point, and as a result, a 1.4% increase in the total-to-static isentropic efficiency was

NOMENCLATURE

ACE	Adaptive Cycle Engine	RFan	Rear fan
CFD	Computational Fluid Dynamics	RVABI	Rear Variable Area Bypass Injector
FFan	Front fan	SST	Shear Stress Transport
HPC	High-Pressure Compressor	$T_{0_{in}}$	inlet total temperature
HPT	High-Pressure Turbine	$T_{0_{ex}}$	outlet total temperature
LPT	Low-Pressure Turbine	T_4	turbine inlet temperature
ISA	International Standard Atmosphere	V	velocity vector
$\dot{m}$	mass flow rate	(u, v, w)	velocity components
MP	mass parameter	β	beta angle
N_L	low-pressure shaft physical speed	$\eta_{is_{tt}}$	total-to-total isentropic efficiency
$P_{0_{in}}$	inlet total pressure	ξ	vorticity vector
$P_{0_{ex}}$	outlet total pressure	γ	heat capacity ratio
PR_{tt}	total-to-total pressure ratio		

achieved. Zhang et al. (2020) applied a three-dimensional multi-point and multi-objective optimization of a centrifugal compressor. By integrating the multi-island GA, the RANS solver, and a data mining method, they performed this process and could increase the efficiency and total pressure ratio by 3% and 5.4%, at the design point, respectively. Ekradi and Madadi (2020) employed the 3D optimization of a centrifugal compressor impeller by using a 3D blade parameterization approach, the genetic algorithm, the ANN, and a computational fluid dynamics solver. The final results indicated that the design point isentropic efficiency was improved by 0.97%. Hosseinimaab and Tousi (2022) optimized the performance parameters of a gas turbine engine by improving its centrifugal compressor geometry. The optimization process was based on three-dimensional numerical simulation, GA, and ANN. Results showed that the engine efficiency and power were increased by 13.93% and 11.07%, respectively, and the specific fuel consumption was reduced by 12.15%. Heidarian Shahri et al. (2024) improved the performance of a centrifugal compressor by investigating the design variables of a cavity squealer tip using the Taguchi method.

The adaptive cycle engine changes key aerodynamic design parameters like pressure ratio and bypass ratio of the engine through geometric structure adjustment, so, it has not only the advantage of large thrust of a low bypass ratio turbofan engine and low fuel consumption of a high bypass ratio engine, but also satisfies the power performance and fuel economy, to achieve the optimal performance. The United States government has tried to complete the development of an adaptive variable cycle engine prototype, to achieve a thrust and fuel efficiency improvement by 10% and 25%, respectively, and, combat radius increment by 25%~30%. In addition, the governments of Britain, France, and Japan have researched adaptive variable cycle engines and achieved remarkable results (Johnson, 1996; Keith et al., 2000; Jimmy et al., 2005; Baughman & Eheart, 2010). The variable cycle compression component is one of the core components of the adaptive variable cycle engine, which is difficult to design and needs to adapt to multiple variable cycle modes and run stably. This paper will carry out an optimal design of the high-pressure compressor of an adaptive cycle engine.

Although improving the performance of simple gas turbine engines (like single-shaft turbojet or turboshaft engines) by optimizing the compressor part is discussed in some papers (Hosseinimaab & Tousi, 2022; Heidarian Shahri et al., 2023), applying this concept to an ACE hasn't been found in the open literature. Also, the available literature on multi-component optimization of centrifugal compressors is limited. Single-component (Zhou et al., 2018) and two-component (Zhang et al., 2018) three-dimensional optimization of centrifugal compressors has been done in previous studies, while 3D three-component optimization (which is implemented in the current research) hasn't been found in the open literature. In the present research, the performance improvement of an adaptive cycle engine is investigated by 3D optimization of the centrifugal compressor used in the engine. First, the configuration and specifications of the ACE and centrifugal compressor are explained, then modeling and optimization methods are described, and finally, a detailed comparison of the performance before and after optimization is presented for both compressor and engine.

2. CASE DESCRIPTION

In the present study, the ACE with the three-stream structure is investigated as the research object. The configuration diagram is presented in Fig. 1, in which the main components are the front fan (FFan), rear fan (RFan), high-pressure compressor (HPC), combustion chamber, high-pressure turbine (HPT), low-pressure turbine (LPT), rear variable area bypass injector (RVABI), afterburner, bypass, and core nozzles. The adaptive fan is coupled with LPT, while the HPC is driven by HPT. This ACE has six variable geometry mechanisms, as shown in Fig. 1, including the inlet guide vanes (IGV) of the RFan, HPT, LPT, RVABI, core, and bypass nozzles.

The HPC of the investigated ACE is a centrifugal compressor consisting of an impeller, radial, and axial diffusers, which is shown in Fig. 2. Some of the main geometrical and performance parameters of the centrifugal compressor are listed in Table 1.

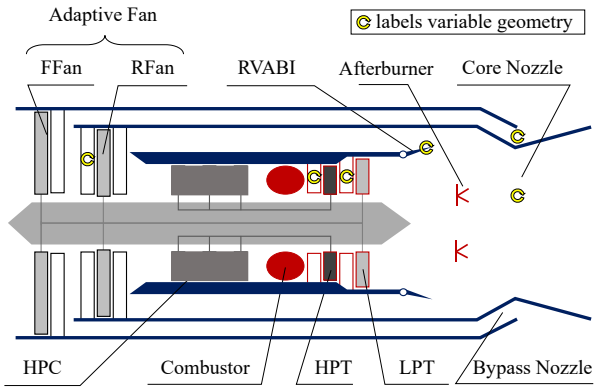

Fig. 1 Configuration of the investigated ACE

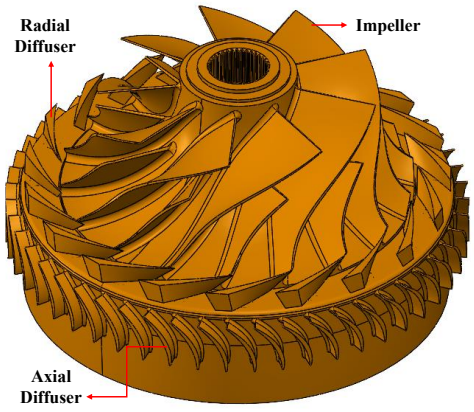

Fig. 2 Three-dimensional geometry of the HPC

Table 1 Geometrical and performance parameters of the HPC

Parameter [Unit]	Value
Impeller blade count (main + splitter)	9+9
Radial diffuser blade count	19
Axial diffuser blade count	51
Hub-to-tip radius ratio at impeller inlet	0.42
Radial diffuser leading edge diameter/impeller diameter	1.02
Height of radial diffuser/impeller diameter	0.06
Height of axial diffuser/impeller diameter	0.04
Design point mass flow rate [kg/s]	2.051
Design point pressure ratio (total-to-total)	4.097

3. METHOD

In this section, the ACE performance simulation method, the CFD simulation method, and the optimization procedure are presented.

3.1 ACE Performance Simulation

One of the most important methods of modeling gas turbine engines is 0D or thermodynamic modeling. This type of modeling is used in many design procedures, such as controller design (Imani & Anjomrouz, 2025), turbomachine design (Saravanamuttoo et al., 2017), etc. The ACE performance simulation program is developed

Table 2 Design point parameters of the ACE

Parameter [Unit]	Value
FFan pressure ratio	1.944
FFan isentropic efficiency	0.829
RFan pressure ratio	1.502
RFan isentropic efficiency	0.860
HPC pressure ratio	4.097
HPC isentropic efficiency	0.743
Turbine inlet temperature (T_4 [K])	1300
Combustion efficiency	0.99
HPT expansion ratio	2.58
HPT isentropic efficiency	0.88
LPT expansion ratio	1.66
LPT isentropic efficiency	0.90
Net thrust (Fn [daN])	333
Specific fuel consumption (SFC [kg/(daN·h)])	0.939

in MATLAB-Simulink software, using the open-source package T-MATS (Chapman et al., 2014). More details of the ACE performance simulation are explained in (Zou, et al., 2024b). In this research, the design point of ACE is chosen to be at sea level and in a static state. The main design point parameters are listed in Table 2, in which the pressure ratios and efficiencies are in total-to-total states.

To validate the 0D performance simulation method, a performance comparison between the T-MATS and test results for a mixed-flow turbofan engine (Zou et al., 2024a) was done and the results (which are normalized by the corresponding test value at the design speed) are shown in Fig. 3. The difference between the T-MATS and test data is less than 2%, which is acceptable for this research.

3.2 CFD Simulation

Three-dimensional, steady state, viscous, and compressible RANS equations are solved by the ANSYS CFX commercial solver. Air ideal gas with variable C_P is used for the working fluid, and the Shear Stress Transport (SST) turbulence model (Menter, 1994) is applied. TurboGrid commercial software is used for mesh generation. Total temperature and pressure are considered as the inlet boundary conditions from the ISA (International Standard Atmosphere), and average static pressure is considered for the outlet boundary condition. The periodic boundary condition is used for lateral faces, and the no-slip condition is for walls. The mixing plane interface is defined between the rotating and stationary domains (Aghaei tog et al., 2008). Some detailed views of the generated mesh for impeller, radial, and axial diffusers, as well as the inlet and outlet boundary conditions, are shown in Fig. 4.

Grid independence check is done by solving the flow field with different mesh sizes from about 700000 to more than 2000000 grid elements, and the main performance parameters are calculated and compared to each other. Normalized values of the pressure ratio, isentropic

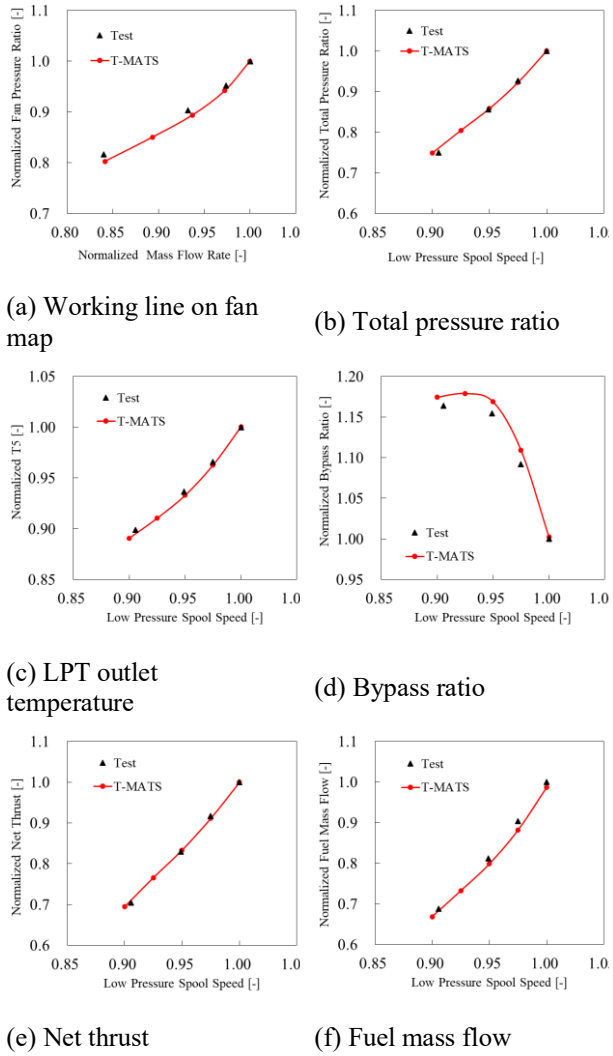

(a) Working line on fan map

(b) Total pressure ratio

(c) LPT outlet temperature

(d) Bypass ratio

(e) Net thrust

(f) Fuel mass flow

Fig. 3 Validation of 0D performance simulation method

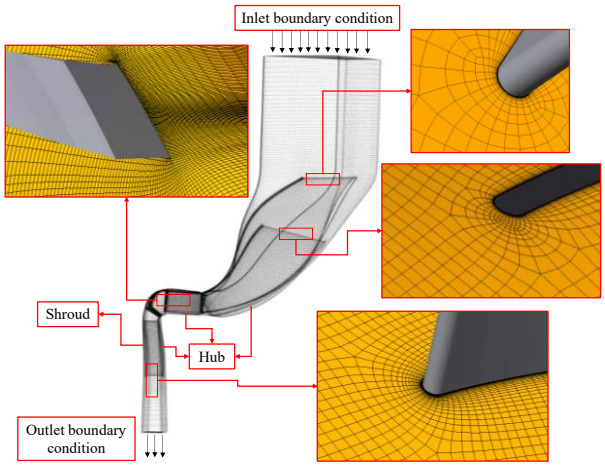

Fig. 4 Details of the generated mesh

efficiency, and mass flow rate versus element number are presented in Fig. 5. A grid with about 1700000 elements has an acceptable accuracy and is chosen for this research.

The CFD simulation method was evaluated on a combined axial-centrifugal compressor by our lab team in

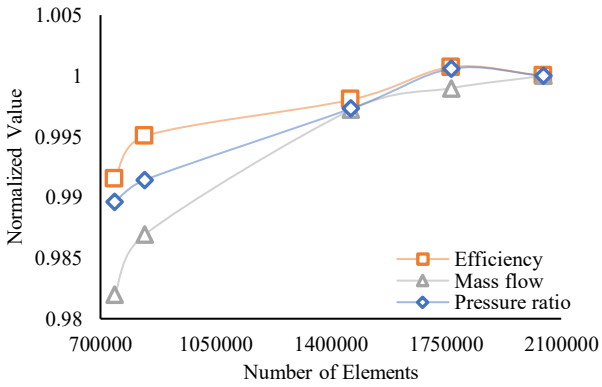

Fig. 5 Grid independence study

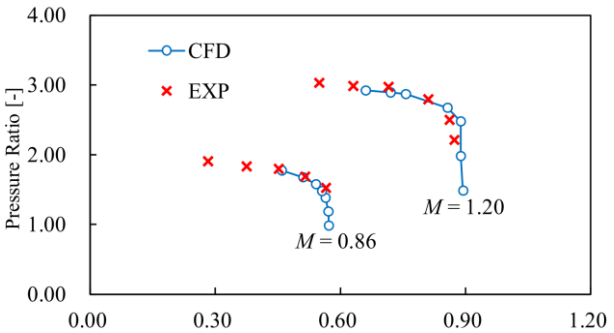

Fig. 6 Validation of CFD simulation method (Li et al., 2023)

the previous research (Li et al., 2023), and the results are presented in Fig. 6. The difference between the CFD results and test data is less than 3%, which is acceptable for the present study. A similar simulation method is used in this research to obtain the steady-state performance of the centrifugal compressor.

3.3 Optimization

In the present study, 3D design point aerodynamic performance optimization of the centrifugal compressor is carried out, and the objective is to maximize the isentropic efficiency by considering a constraint on the total pressure ratio. The definition of this optimization problem is as follows ($f(x)$ is the objective function and $g(x)$ is the constraint):

$$\text{Maximize } f(x) = \eta_i$$

$$\text{subject to} \quad (1)$$

$$g(x) \leq 0$$

In which:

$$g(x) = 4 - PR_t \quad (2)$$

There are many parameters affecting the centrifugal compressor geometry and performance, including meridional curves of hub and shroud, blade camber line, thickness distribution, blade count, etc. Considering these parameters for the impeller, radial and axial diffusers form a large (high-dimensional) design space; but for an optimization problem, it's not necessary to change all the geometrical parameters, and sometimes it's suitable to

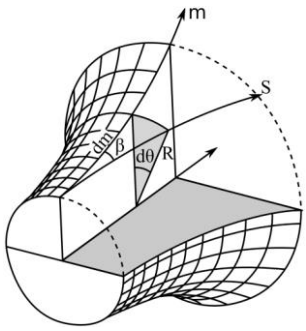

Fig. 7 Camber line definition by Beta angle (Verstraete, 2010)

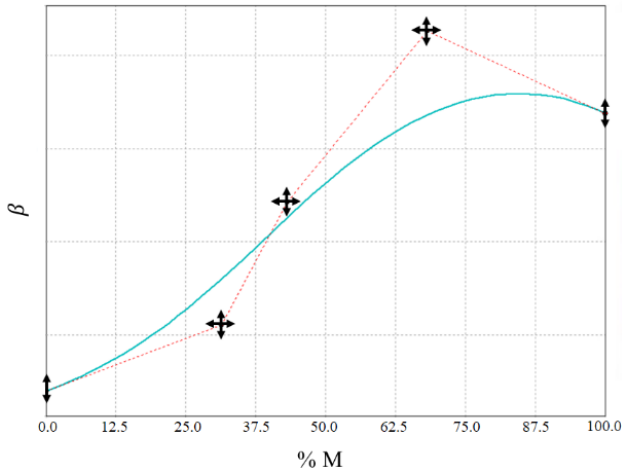

Fig. 8 Beta angle distribution by the Bezier curve modeling

reach the optimized geometry with minimum parameters to have less computational cost.

In this research, the blade camber line is selected as the design variable. Camber line is defined by the $\beta(u)$ angle distribution between the meridional direction m and the streamline S (Fig. 7) in which $u \in [0,1]$ is the non-dimensional meridional length, has a value of 0 at the leading edge and 1 for the trailing edge. The camber line circumferential position θ is defined as follows and allows the transformation from the β domain to the Cartesian coordinate.

$$R\, d\theta = dm \tan(\beta) \tag{3}$$

The beta angle (β) of the impeller, radial, and axial diffusers is selected as a design variable. A fourth-order Bezier curve with five control points is selected to define the β angle distribution in the hub and shroud. Also, β_0 to β_4 are the analogous angles for the leading edge to the trailing edge.

$$\begin{aligned}\beta(u) = \beta_0(1-u)^4 + 4\beta_1 u(1-u)^3 \\ + 6\beta_2 u^2(1-u)^2 \\ + 4\beta_3 u^3(1-u) + \beta_4 u^4\end{aligned} \tag{4}$$

The coordinates of the Bezier curves' control points are chosen as the design variables that should be changed to optimize the objective function. The possible variations of the Bezier curves' control points are presented in Fig. 8, by the arrow. The inlet blade angle of the impeller main blade and the outlet blade angle of the axial diffuser are fixed from the base geometry for better matching between the optimized geometry with other parts of the engine.

An experiment involves conducting tests or a series of runs where desired changes are applied to the input variables of a system. This is done to identify the reasons for any changes that may occur in the output response. Fitting response surfaces is greatly aided by the suitable selection of an experimental design. In recent years, different space-filling designs have been proposed. One such method is the Latin Hypercube Sampling (LHS) design (Montgomery, 2017).

The Kriging method was first developed in 1960 by D. G. Krige, a South African engineer, for mining applications and later adopted for optimization purposes. The model uses input responses to fit a curve based on regression analysis. This can be expressed as equation (5), in which the known function $f(x)$ shows the trend over the design space and the unknown function $F(x)$ is to be estimated. The function $Z(x)$ creates a localized deviation to interpolate the sampled data with a Gaussian connection (Kim et al., 2019).

$$F(x) = f(x) + Z(x) \tag{5}$$

In this research, samples are produced by the LHS, and then the Kriging method is used to make a surrogate model based on the three-dimensional CFD simulation results that have been done for the generated samples. In this step, each sample is also checked to reach desired objectives.

The optimization problem of the present study is nonlinear, constrained, and has a large number of local optimums so the nondominated sorting genetic algorithm II (NSGA II) (Deb et al., 2002), which is a fast and elitist evolutionary algorithm, is applied as a modern optimizer to solve the optimization problem. The general flowchart of the proposed optimization process is observed in Fig. 9. According to this figure, a surrogate model-assisted optimization method is applied in this study. The optimization algorithm is applied to the surrogate model generated by Kriging to accelerate the optimization process, and the final CFD calculation of the optimal design certifies the accuracy of the results.

4. RESULTS AND DISCUSSION

The centrifugal compressor optimization results are presented in this section, and then, the ACE performance is evaluated before and after the optimization. The mass parameter, total-to-total pressure ratio, and isentropic efficiency, which are used in the results, are calculated from the following equations, respectively (Saravanamuttoo et al., 2017).

$$MP = \dot{m}\frac{\sqrt{T_{0_{in}}}}{P_{0_{in}}} \tag{6}$$

$$PR_{tt} = \frac{P_{0_{ex}}}{P_{0_{in}}} \tag{7}$$

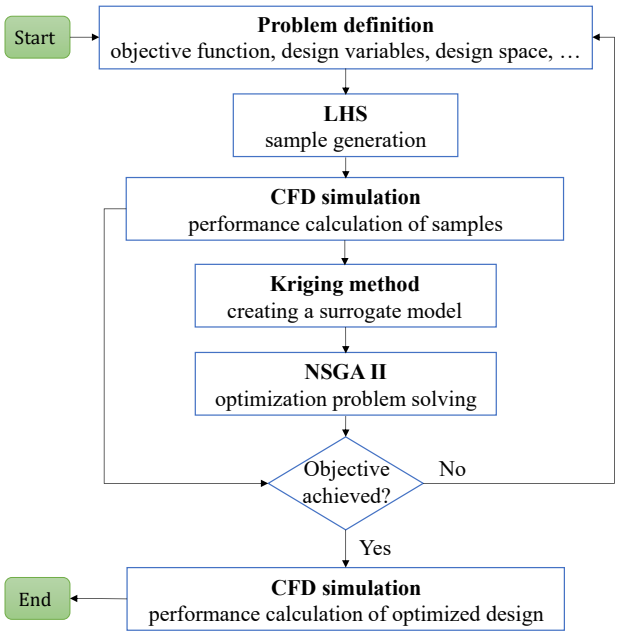

Fig. 9 Optimization process flowchart

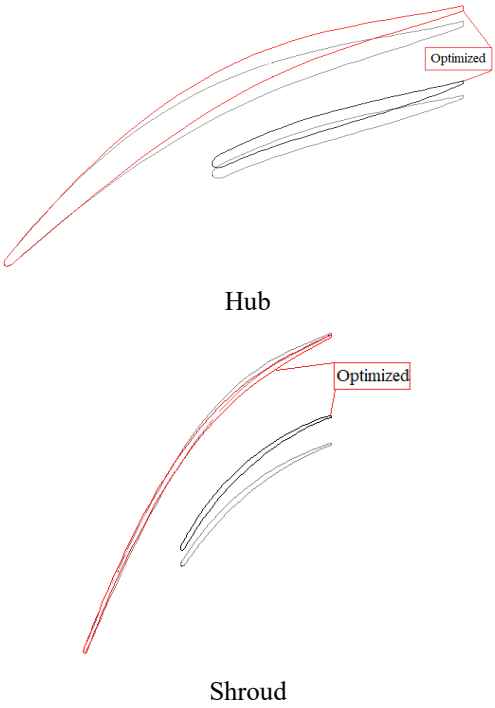

Fig. 10 Impeller blade profile in hub and shroud before and after optimization

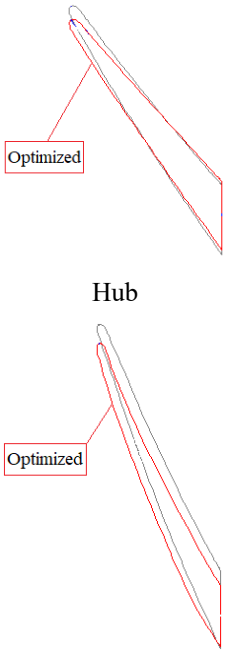

Fig. 11 Radial diffuser blade profile in hub and shroud before and after optimization

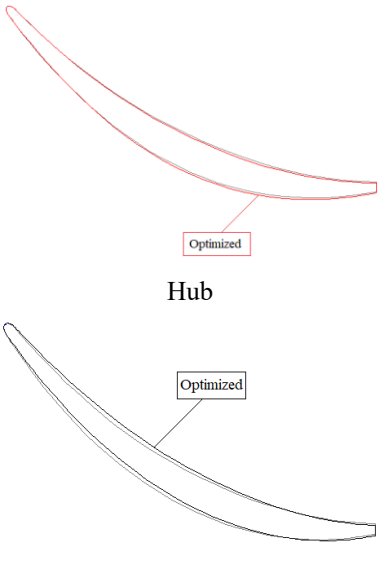

Fig. 12 Axial diffuser blade profile in hub and shroud before and after optimization

$$\eta_{is_{tt}} = \frac{PR_{tt}^{\frac{\gamma-1}{\gamma}} - 1}{\frac{T_{0_{ex}}}{T_{0_{in}}} - 1} \tag{8}$$

4.1 Compressor Optimization Results

In this section, first, the geometrical changes of the impeller, radial, and axial diffusers are presented. As stated before, no change has been made in the inlet angle of the impeller main blade and the axial diffuser outlet blade angle. Both optimized and base geometries are plotted in the same figure to show the changes for the hub and shroud during the optimization process in Fig. 10. to Fig. 12. A 3D view of the impeller blade is shown in Fig. 13. before and after optimization, in which the black color is used for the base geometry.

The three-dimensional view of the impeller blade is shown in Fig. 13 before and after optimization, in which the black color is used for the base geometry. This figure shows 3D geometrical changes in the impeller blade through optimization and clarifies that the splitter blade has experienced more changes than the main blade.

Fig. 13 3D view of the impeller blade before and after optimization

Table 3 Design point performance parameters for the base and optimized compressors

Parameter [unit]	Base	Optimized	Base and optimized difference (%)
Mass flow rate [kg/s]	2.051	2.102	2.5
Total pressure ratio	4.097	4.091	0.1
Isentropic efficiency	0.743	0.768	3.4

A comparison has been made between the design point performance parameters of the base and optimized compressor, and the results are shown in Table 3. For the optimized compressor, although the design point total pressure ratio is decreased by 0.1%, the isentropic efficiency is increased by 3.4%. Also, the mass flow rate is increased by about 2.5%.

For further investigation, the characteristic lines at design speed are calculated for both optimized and base compressors and are presented in Fig. 14 and Fig.15 for the total-to-total pressure ratio and isentropic efficiency, respectively. According to these figures, the choked mass flow rate of the optimized compressor is 1.4% higher than the base case and provides a wider operating range. For the same mass flow rate, the total pressure ratio and isentropic efficiency of the optimized compressor are higher than the base one.

For a detailed investigation, some of the flow characteristics are presented and compared in both optimized and base geometries. One such characteristic is the vorticity. It's defined as the curl of the velocity field and is calculated from the following equations, in which V is the velocity vector, (u, v, w) are its components, and ξ is the vorticity vector (White, 2021).

$$V(x,y,z) = \mathrm{i}u(x,y,z) + \mathrm{j}v(x,y,z) + \mathrm{k}w(x,y,z) \tag{9}$$

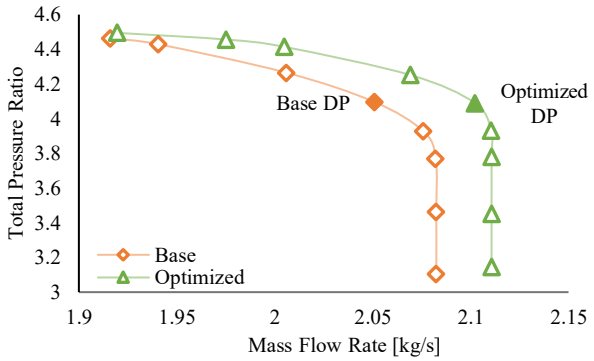

Fig. 14 Total-to-total pressure ratio performance line of the optimized and base compressors at the design speed

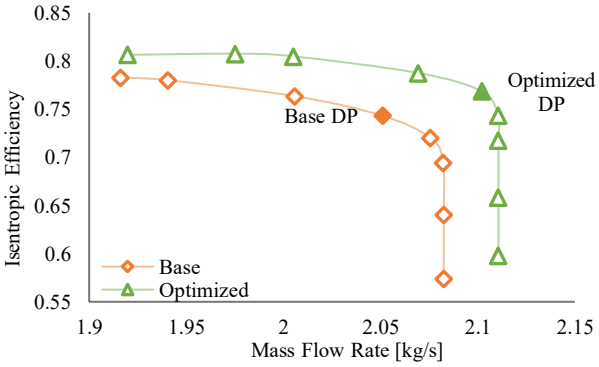

Fig. 15 Total-to-total isentropic efficiency performance line of the optimized and base compressors at the design speed

$$\xi = \mathrm{curl}\, V = \nabla \times V = \begin{vmatrix} \mathrm{i} & \mathrm{j} & \mathrm{k} \\ \frac{\partial}{\partial x} & \frac{\partial}{\partial y} & \frac{\partial}{\partial z} \\ u & v & w \end{vmatrix} \tag{10}$$

$$\xi = \mathrm{i}\left(\frac{\partial w}{\partial y} - \frac{\partial v}{\partial z}\right) + \mathrm{j}\left(\frac{\partial u}{\partial z} - \frac{\partial w}{\partial x}\right) + \mathrm{k}\left(\frac{\partial v}{\partial x} - \frac{\partial u}{\partial y}\right) \tag{11}$$

The velocity streamlines for the base and optimized geometries are presented in Fig.16 and Fig.17 in the blade-to-blade view for two spans. Near the hub region, there are vortical flows in both optimized and base compressors. For example, in the 0.05 span, there is a vortical region in the axial diffuser inlet of the base compressor and a smaller one in the axial diffuser outlet of the optimized compressor. For the base case, the vortical flow region transfers from the inlet to the outlet of the axial diffuser and increases for spans of upper than 0.5, but in the optimized compressor, the vortical flow region is decreased for upper spans, and there is no vortex in the near shroud region. According to Fig. 17, the vortical flow region in the optimized compressor is eliminated for the 0.95 span, but in the base geometry, there are some vortices at the axial diffuser outlet. Also, the separation zone near the outlet of the impeller passage (which is

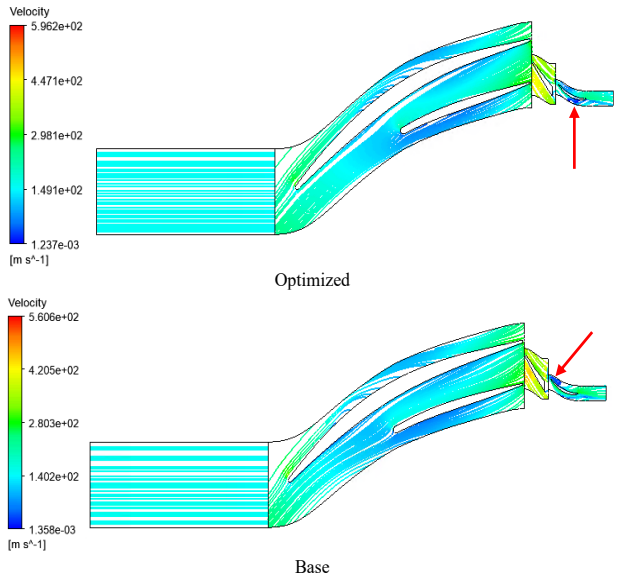

Fig. 16 Velocity streamlines in blade-to-blade view for the optimized and base geometries at 0.05 span

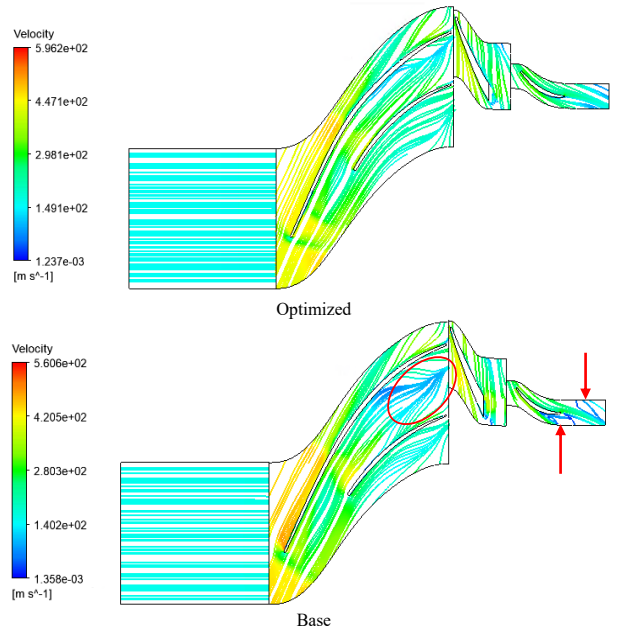

Fig. 17 Velocity streamlines in blade-to-blade view for the optimized and base geometries at 0.95 span

shown in Fig. 17 with a red oval) is reduced in the optimized compressor.

The relative Mach number contours of the compressors in meridional view are compared in Fig. 18. According to this figure, in the impeller region, the relative Mach number has a more uniform distribution and reaches a higher value at the impeller outlet in the optimized geometry. This causes a better impeller performance.

Similar to the relative Mach number contour, the pressure distribution is more uniform in the impeller region of the optimized geometry (Fig. 19).

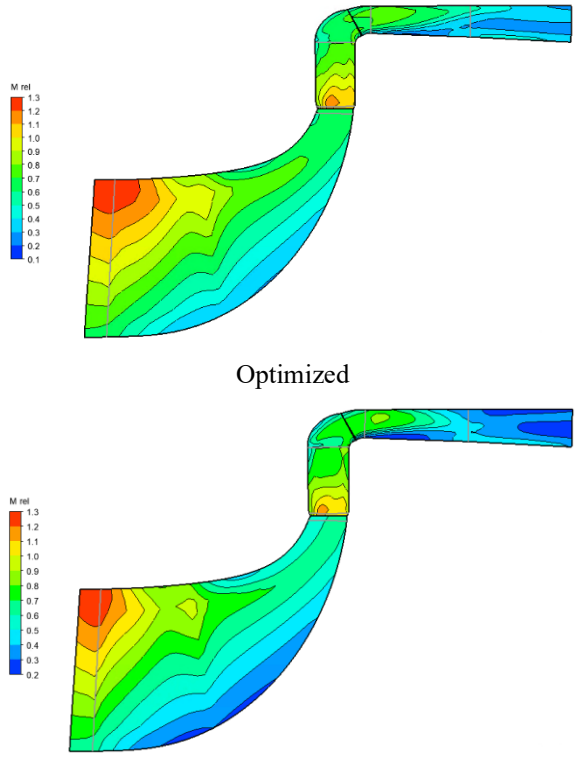

Fig. 18 Relative Mach number contour in meridional view for the optimized and base geometries

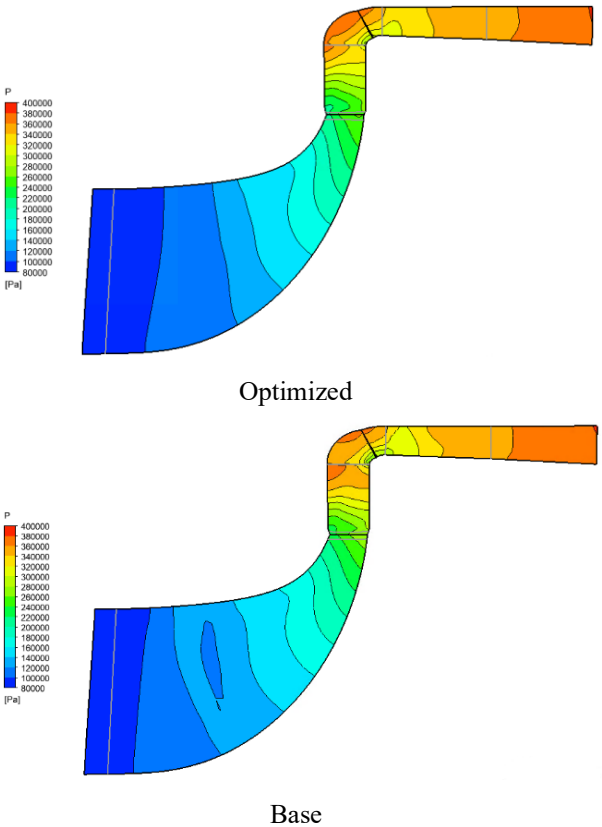

Fig. 19 Pressure contour in meridional view for the optimized and base geometries

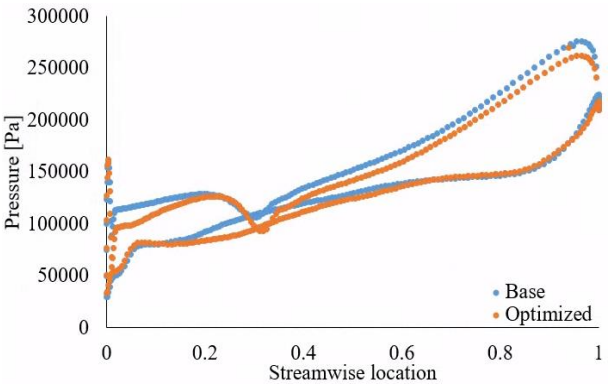

Fig. 20 Blade loading of impeller main blades at 0.5 span

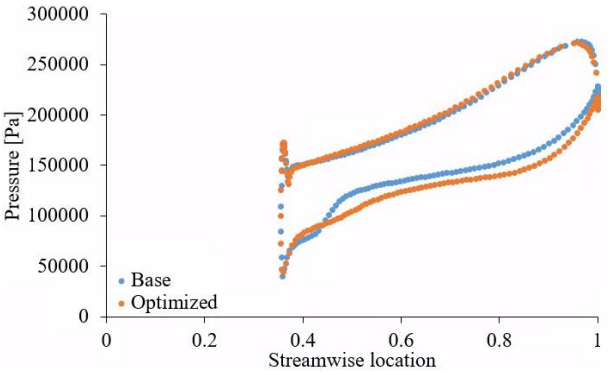

Fig. 21 Blade loading of impeller splitter blades at 0.5 span

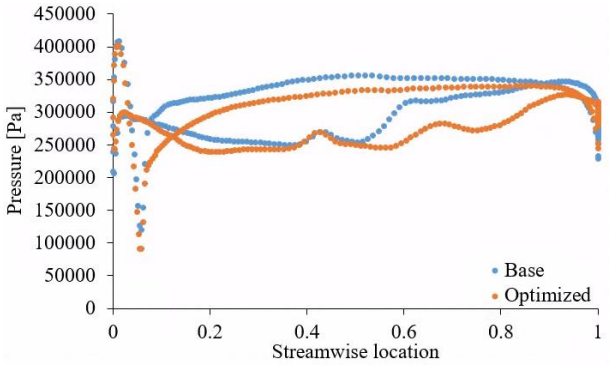

Fig. 22 Blade loading of radial diffuser blades at 0.5 span

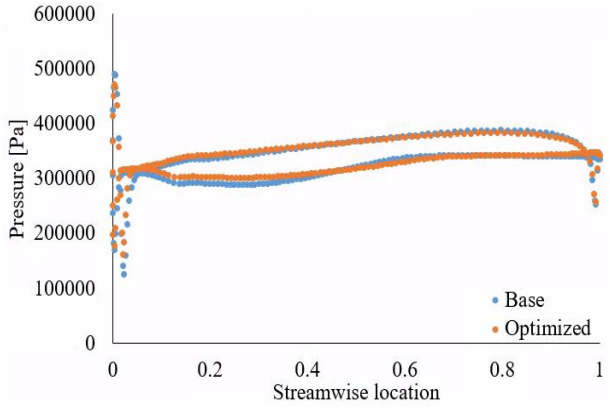

Fig. 23 Blade loading of axial diffuser blades at 0.5 span

The pressure distribution on the blade surfaces (suction and pressure sides) in the impeller, radial, and axial diffusers is presented as follows for the optimized and base geometries. The minimum difference between the blade loading before and after optimization occurs in the axial diffuser (Fig. 23). For the radial diffuser (Fig. 22), the pressure value on the base blade (on both pressure and suction sides) is generally higher than the optimized blade. In the impeller section (Fig. 20 and Fig. 21), the behavior is more complex but it is generally observed that, in the splitter blades, the pressure value on the suction side of the base geometry is higher than the optimized geometry and for the main blades, the pressure value on the pressure side of the base geometry is higher than the optimized one.

4.2 Engine Performance Results

The engine performance improvements are illustrated by comparing the key parameters of the base and improved ACEs. By considering the turbine inlet temperature (T_4) as the engine control variable and fixing it in the base and improved engines, it's possible to have a comparison between the base and improved engines. The comparison results for this case are presented in Table 4. According to this table, the SFC is decreased by 0.3% for the improved engine, and the net thrust and normalized N_L are increased by 0.9% and 2.0%, respectively.

Table 4 Design point performance parameters for the base and improved ACEs with T_4 constant

Parameter [unit]	Base	Improved	Base and improved difference (%)
SFC [kg/(daN·h)]	0.939	0.936	0.3
F_n [daN]	333	336	0.9
Normalized N_L	1.00	1.02	2.0

In the present research, the low-pressure shaft physical speed N_L is mainly chosen as the engine control variable. By this selection, N_L is constant in the base and improved ACEs. It should be noted that other results of this research are presented for this case. For this situation, a comparison of some main performance characteristics of the base and improved engines at the design point is presented in Table 5. According to this table, the SFC, net thrust, and turbine inlet temperature of the improved engine are decreased by 2.0%, 2.1%, and 2.4%, respectively. The thrust reduction of the improved engine is reasonable because of the reduction in T4, which is an important parameter for the net thrust. The lower turbine inlet temperature can also increase the turbine blade lifetime for the reduction of thermal loading.

Table 5 Design point performance parameters for the base and improved ACEs with N_L constant

Parameter [unit]	Base	Improved	Base and improved difference (%)
SFC [kg/(daN·h)]	0.939	0.920	2.0
F_n [daN]	333	326	2.1
T_4 [K]	1300	1269	2.4

Table 6 Design point performance parameters for the base and improved ACEs with F_n constant

Parameter [unit]	Base	Improved	Base and improved difference (%)
SFC [kg/(daN·h)]	0.939	0.931	0.9
T_4 [K]	1300	1290	0.8
Normalized N_L	1.00	1.02	2.0

Another comparison between the base and improved ACEs is performed at fixed thrust. From Table 6, it's observed that the SFC and T_4 are decreased by 0.9% and 0.8%, respectively, while N_L is increased by 2.0%. This shows the benefit of SFC reduction is also available at fixed thrust.

The performance of the base and optimized compressors and engines is investigated at the design point in the previous sections of this research. Now the performance is investigated for off-design conditions. In Fig. 24, the specific fuel consumption is plotted versus the net thrust for the base and improved engines on the working line. It is observed that for the same thrust, the SFC of the improved ACE is lower than the base engine, which is an important achievement of this research.

The ACEs working lines on the total pressure ratio and isentropic efficiency performance maps of the centrifugal compressor are presented in Fig. 25 and Fig. 26, respectively. Results show that the improved engine working line has a lower pressure ratio and higher efficiency than the base case, for the same mass flow rate.

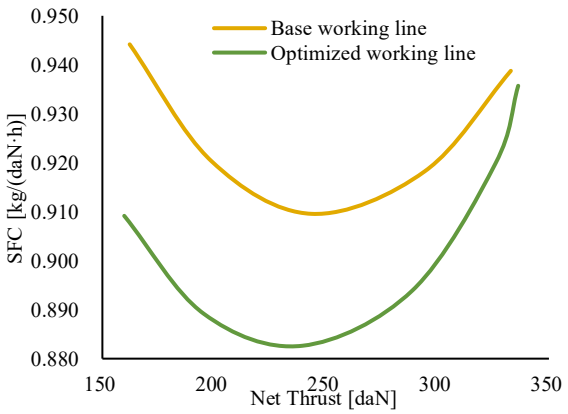

Fig. 24 SFC versus net thrust of the base and improved engines

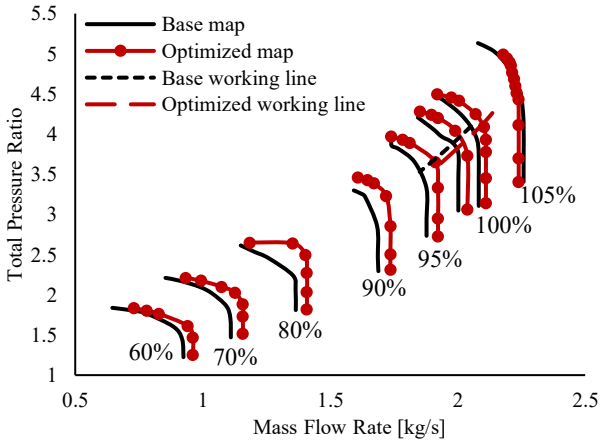

Fig. 25 Total pressure ratio performance map of the HPC with the engine working line

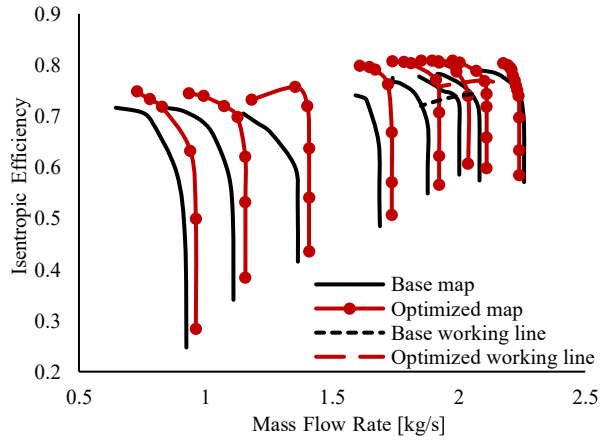

Fig. 26 Isentropic efficiency performance map of the HPC with the engine working line

5. CONCLUSION

Nowadays, many researchers are focused on various aspects of adaptive cycle engines because of the important capabilities of these engines. In the ACEs, some aerodynamic parameters, such as bypass and pressure ratio, can change by geometric structure adjustment. This paper aimed to improve the performance of the ACE by aerodynamic optimization of its HPC. A three-dimensional surrogate-assisted method is applied for the aerodynamic optimization of the centrifugal compressors at the design point to maximize the efficiency with a constraint on the total pressure ratio. The optimization results showed good achievements in the compressor performance. The isentropic efficiency was increased by 3.4% while the total pressure ratio was decreased by 0.1% at the design point. Also, the compressor operating range became wider, and the choked mass flow rate was increased by 1.4% through optimization.

After that, the performance simulation of the ACE was done by the 0D modeling method in combination with the performance map obtained by 3D CFD simulation. By fixing T_4 between the base and improved engines, the SFC was decreased by 0.3%, and the net thrust was increased

by 0.9% for the improved engine. Also, by choosing the N_L as the engine control variable and fixing it between the base and improved engines, the specific fuel consumption and net thrust decreased by 2.0% and 2.1%, respectively.

For future work related to this research, it is recommended to apply the optimization method on both FFan and RFan to achieve better performance for the adaptive fan as well as the whole engine.

CONFLICT OF INTEREST

The author declares no conflicts of interest.

ACKNOWLEDGMENT

The first author wants to thank the assistance received from Dr. Ali Hajilouy Benisi and Dr. Mohamad Sadeq Karimi.

AUTHORS CONTRIBUTION

A. Anjomrouz: Conceptualization, Software, Investigation, Methodology, Writing – original draft, Writing – review & editing. **W. Zou**: Software, Methodology, Writing – original draft, Writing – review & editing. **W. Kong**: Writing – original draft, Writing – review & editing. **B. Wang**: Methodology, Writing – review & editing. **X. Zheng**: Supervision, Project administration.

REFERENCES

Aghaei tog, R., Tousi, A. M., & Tourani, A. (2008). Comparison of turbulence methods in CFD analysis of compressible flows in radial turbomachines. *Aircraft Engineering and Aerospace Technology, 80*(6), 657-665. https://doi.org/10.1108/00022660810911608

Anjomrouz, A., Ghadiri, S., & Imani, A. (2023). A review on the structures and characteristics of micro-turbojet engines. *Journal of Solid and Fluid Mechanics, 13*(5), 59-76. https://doi.org/10.22044/jsfm.2023.13523.3780

Baughman, J. L., & Eheart, R. (2010). *Aft fan adaptive cycle engine*. G. E. Company. https://patents.google.com/patent/US20120131902A1/en

Chapman, J. W., Lavelle, T. M., May, R. D., Litt, J. S., & Guo, T. H. (2014). *Toolbox for the modeling and analysis of thermodynamic systems (T-MATS) user's guide*. https://ntrs.nasa.gov/citations/20140012486

Cheng, J., Jiang, C., & Xiang, H. (2019). A surface parametric control and global optimization method for axial flow compressor blades. *Chinese Journal of Aeronautics, 32*(7), 1618-1634. https://doi.org/10.1016/j.cja.2019.05.002

Deb, K., Pratap, A., Agarwal, S., & Meyarivan, T. (2002). A fast and elitist multiobjective genetic algorithm: NSGA-II. *IEEE Transactions on Evolutionary Computation, 6*(2), 182-197. https://doi.org/10.1109/4235.996017

Ekradi, K., & Madadi, A. (2020, 2020/06/15/). Performance improvement of a transonic centrifugal compressor impeller with splitter blade by three-dimensional optimization. *Energy, 201*, 117582. https://doi.org/https://doi.org/10.1016/j.energy.2020.117582

Hehn, A., Mosdzien, M., Grates, D., & Jeschke, P. (2018). Aerodynamic optimization of a transonic centrifugal compressor by using arbitrary blade surfaces. *Journal of Turbomachinery, 140*(5), 051011. https://doi.org/10.1115/1.4038908

Heidarian Shahri, M., Habibzadeh, S., Madadi, A., & Benini, E. (2024). Investigation of aerodynamic effects and dominant design variables of cavity squealer-tip in three-dimensional performance of a centrifugal compressor. *Aerospace Science and Technology, 152*, 109382. https://doi.org/https://doi.org/10.1016/j.ast.2024.109382

Heidarian Shahri, M., Madadi, A., & Boroomand, M. (2023). Three-Dimensional optimization of blade lean and sweep for an axial compressor to improve the engine performance. *Journal of Applied Fluid Mechanics, 16*(11), 2206-2218. https://doi.org/10.47176/jafm.16.11.1857

Hosseinimaab, S., & Tousi, A. (2022). Optimizing the performance of a single-shaft micro gas turbine engine by modifying its centrifugal compressor design. *Energy Conversion and Management, 271*, 116245. https://doi.org/10.1016/j.enconman.2022.116245

Imani, A., & Anjomrouz, A. (2025). Design and Simulation of a control system for a single spool mixed-flow small turbofan engine. *Journal of Aeronautics, Astronautics and Aviation, 57*(1), 1-12. https://doi.org/10.6125/JoAAA.202501_57(1).01

Johnson, J. E. (1996). Variable cycle engine developments at general electric-1955-1995. *Developments In High-Speed Vehicle Propulsion Systems* (pp. 105-158). https://doi.org/10.2514/5.9781600866401.0105.0158

Jimmy, T., Bryce, R., & Dimitri, M. (2005). Development of an NPSS variable cycle engine model. *ISABE, 1295*. https://api.semanticscholar.org/CorpusID:185503294

Keith, B. D., Basu, D. K., & Stevens, C. (2000). *Aerodynamic test results of controlled pressure ratio engine (COPE) dual spool air turbine rotating rig.* ASME Turbo Expo 2000: Power for Land, Sea, and Air. https://doi.org/10.1115/2000-GT-0632

Kim, K. Y., Samad, A., & Benini, E. (2019). *Design Optimization of Fluid Machinery: Applying Computational Fluid Dynamics and Numerical Optimization*. John Wiley & Sons. https://doi.org/10.1002/9781119188377

Li, J., Wen, M., Wang, B., & Zheng, X. (2023). *Investigation on the unsteady surge flow behavior of an axial-centrifugal compressor.* Turbo Expo: Power for Land, Sea, and Air. https://doi.org/10.1115/GT2023-103407

Menter, F. R. (1994). Two-equation eddy-viscosity turbulence models for engineering applications. *AIAA Journal, 32*(8), 1598-1605. https://doi.org/10.2514/3.12149

Mojaddam, M., & Moussavi Torshizi, S. A. (2017). Design and optimization of meridional profiles for the impeller of centrifugal compressors. *Journal of Mechanical Science and Technology, 31*(10), 4853-4861. https://doi.org/10.1007/s12206-017-0933-3

Mojaddam, M., & Pullen, K. R. (2019). Optimization of a Centrifugal compressor using the design of experiment technique. *Applied Sciences, 9*(2), 291. https://doi.org/10.3390/app9020291

Montgomery, D. C. (2017). *Design and Analysis of Experiments* (9th ed.). John Wiley & Sons. https://www.wiley.com/Design+and+Analysis+of+Experiments%2C+EMEA+Edition%2C+9th+Edition-p-9781119638421

Nili-Ahmadabadi, M., & Poursadegh, F. (2013a, 2013/03/01). Centrifugal compressor shape modification using a proposed inverse design method. *Journal of Mechanical Science and Technology, 27*(3), 713-720. https://doi.org/10.1007/s12206-013-0120-0

Nili-Ahmadabadi, M., & Poursadegh, F. (2013b, 2013/11/01). Optimization of a seven-stage centrifugal compressor by using a quasi-3D inverse design method. *Journal of Mechanical Science and Technology, 27*(11), 3319-3330. https://doi.org/10.1007/s12206-013-0854-8

Saravanamuttoo, H. I. H., Rogers, G. F. C., Cohen, H., Straznicky, P., & Nix, A. (2017). *Gas Turbine Theory*. Pearson. https://books.google.com/books?id=4AH-MAAACAAJ

Verstraete, T. (2010). *CADO : a computer aided design and optimization tool for turbomachinery applications.* 2nd International Conference on Engineering Optimization, Lisbon, Portugal. http://www1.dem.ist.utl.pt/engopt2010/Book_and_CD/Papers_CD_Final_Version/pdf/01/01297-01.pdf

White, F. M. (2021). *Fluid mechanics* (9th ed.). The McGraw Hill Companies. https://www.mheducation.com/highered/product/fluid-mechanics-white.html

Xiang, H., Chen, J., Cheng, J., Niu, H., Liu, Y., & Song, X. (2021). Aerodynamic improved design and optimization for the rear stage of a High-load axial compressor. *Journal of the Brazilian Society of Mechanical Sciences and Engineering, 43*, 1-20. https://doi.org/10.1007/s40430-021-02848-2

Zangeneh, M., Goto, A., & Harada, H. (1999). On the role of three-dimensional inverse design methods in turbomachinery shape optimization. *Proceedings of the Institution of Mechanical Engineers, Part C: Journal of Mechanical Engineering Science, 213*(1), 27-42. https://doi.org/10.1243/0954406991522167

Zhang, L., Mi, D., Yan, C., & Tang, F. (2018). Multidisciplinary design optimization for a centrifugal compressor based on proper orthogonal decomposition and an adaptive sampling method. *Applied Sciences, 8*(12), 2608. https://doi.org/10.3390/app8122608

Zhang, Y., Xu, S., & Wan, Y. (2020). Performance improvement of centrifugal compressors for fuel cell vehicles using the aerodynamic optimization and data mining methods. *International Journal of Hydrogen Energy, 45*(19), 11276-11286. https://doi.org/10.1016/j.ijhydene.2020.02.026

Zhou, L., Xiang, F., & Wang, Z. (2018). CFD Investigation on the application of optimum non-axisymmetric endwall profiling for a vaned diffuse. *Journal of Applied Fluid Mechanics, 11*(6), 1703-1715. https://doi.org/10.29252/jafm.11.06.28664

Zou, W., Song, Z., Wang, B., Wen, M., & Zheng, X. (2024a). An efficient multi-fidelity simulation approach for performance prediction of adaptive cycle engines. *Journal of the Global Power and Propulsion Society, 8*, 310-322. https://doi.org/10.33737/jgpps/191167

Zou, W., Zheng, X., Liu, W., Lai, J., & Wang, B. (2024b). 0D-1D coupled method for performance design and analysis of adaptive cycle engine - Modeling, simulation and validation. *Energy, 313*, 133666. https://doi.org/https://doi.org/10.1016/j.energy.2024.133666